Branched actin networks in innate immune cells mediate host microbiota homeostasis.

Luiz Ricardo C. Vasconcellos[1,†], Shaina Chor Mei Huang[1,†], Alejandro Suarez-Bonnet[2, 3], Simon Priestnall[2, 3], Sunita Varsani-Brown[4], Matthew L. Winder[4], Kathleen Shah[5], Naoko Kogata[1], Brigitta Stockinger[5], Michael Way[1,6]

[1] Cellular Signalling and Cytoskeletal Function Laboratory, The Francis Crick Institute, 1 Midland Road, London, NW1 1AT, UK.

[2] Experimental Histopathology, The Francis Crick Institute, 1 Midland Road, London, NW1 1AT, UK.

[3]Department of Pathobiology and Population Sciences, Royal Veterinary College, Hatfield Hertfordshire, AL9 7TA, UK.

[4]Genetic Modification Service, The Francis Crick Institute, 1 Midland Road, London, NW1 1AT, UK.

[5]AhR Immunity Laboratory, The Francis Crick Institute, 1 Midland Road, London, NW1 1AT, UK.

[6]Department of Infectious Disease, Imperial College, London W2 1PG, UK

† These authors contributed equally to this work

Abstract:

Assembly of branched actin networks, driven by the Arp2/3 complex are essential for the function and integrity of the immune system. Patients with loss-of-function mutations in the ARPC5 subunit of the Arp2/3 complex develop inflammation and immunodeficiency after birth, leading to early mortality. However, the mechanistic basis for these phenotypes remains obscure. Here we demonstrate that loss of Arpc5 in the murine hematopoietic system, but not the corresponding Arpc5l isoform causes early-onset intestinal inflammation. This condition is initiated by microbiota breaching the ileal mucosa, leading to local and systemic inflammation. Macrophage and neutrophils infiltrate into the ileum, but in the absence of Arpc5 fail to restrict microbial invasion. Loss of Arpc5 compromises the ability of macrophages to phagocytose and kill intra-cellular bacteria. Our results underscore the indispensable role of Arpc5, but not Arpc5l containing Arp2/3 complexes in mononuclear phagocytes function and host-microbiota homeostasis.

One-Sentence Summary:

Arpc5 containing Arp2/3 complexes are essential for host-microbiota homeostasis

Introduction

Mutations in genes encoding proteins involved in the regulation and organization of the actin cytoskeleton frequently result in primary immunodeficiency (*1*). These so-called actinopathies have a wide spectrum of severity involving the innate and/or the adaptive arm of the immune system (*2*). The most well-known actinopathy, Wiskott-Aldrich Syndrome (*3*), is caused by mutations in WASP, a hematopoietic specific protein that activates the Arp2/3 complex to nucleate branched actin filament networks (*4, 5*). A functioning immune system depends on these networks to drive cell migration, phagocytosis and immunological synapse assembly (*6, 7*). The Arp2/3 complex consists of seven evolutionarily conserved subunits, two Actin Related Proteins: Arp2, Arp3 and ArpC1-ArpC5 (*8, 9*). However, in mammals, three of the subunits have two different isoforms (Arp3/Arp3B, ARPC1A/ARPC1B and ARPC5/ARPC5L), each of which confers different properties to the Arp2/3 complex (*10-12*). The importance of these subunit isoforms is underscored by the observation that mutations in human ARPC1B result in severe immunodeficiency as well as impaired cytotoxic T lymphocyte maintenance and activity (*13-16*).

More recently, loss of function mutations in ARPC5 have also been reported to result in gastrointestinal conditions, increased susceptibility to infection leading to sepsis and early death (*17, 18*). The mechanistic basis for these clinical observations in patients with ARPC5 mutations remains unknown. We therefore examined the impact of the loss of Arpc5 in the murine hematopoietic compartment to determine the basis for these immune phenotypes.

Loss of Arpc5 in immune cells leads to spontaneous enteritis

As ubiquitous loss of Arpc5 in mice is embryonic lethal (*18*), we used the Vav1-iCre driver (*19*), to delete Arpc5 in the hematopoietic compartment (Fig.1A, fig. S1A). At 8-15 weeks of age, *Arpc5*$^{fl/fl_Vav1Cre+}$ animals (hereafter referred to as C5$^{\Delta Vav}$) had reduced weight gain and increased levels of faecal lipocalin-2, a marker of intestinal inflammation (*20*), compared to littermate controls (C5$^{fl/fl}$ and C5^{HetVav}) (Fig.1B, fig. S1B). Consistent with this, adult C5$^{\Delta Vav}$ had intestinal inflammation with increased infiltration of macrophages and neutrophils, and loss of structural integrity, which was not seen in control mice (Fig.1C and D, fig. S1C). The inflammation and damage was restricted to the ileum of the small intestine (Fig.1D, fig. S1D). The mesenteric (mLNs) but not the inguinal lymph nodes (iLNs) were enlarged (Fig.1E), indicating a local immune response in the intestine. The increase in size of mLNs was driven by an expansion of lymphocytes and a dramatic recruitment of neutrophils and macrophages (fig. S1E). Importantly, no inflammation or intestinal damage were observed in age matched *Arpc5l*$^{fl/fl_Vav1Cre+}$ (C5L$^{\Delta Vav}$) animals (fig. S1F and G). Our observations demonstrate that Arpc5 but not the alternative Arpc5l isoform is essential for maintenance of intestinal homeostasis by the immune system.

Arpc5 deficiency leads to systemic inflammation

Assessing the severity of inflammation, we found that C5$^{\Delta Vav}$ mice had increased serum levels of C-reactive protein (CRP), a marker of inflammation (Fig.1F). The number of neutrophils and monocytes in the blood of C5$^{\Delta Vav}$ mice increased, while only CD4 T cells decreased (Fig.1G and fig. S1H). Similar changes in cell numbers in the peripheral blood were reported in patients lacking ARPC5 (*17*). C5$^{\Delta Vav}$ mice also had pale bone marrow due to a reduction in erythroid lineages and an increase in Ly6G^{lo} immature neutrophils (Fig.1H), as observed in mice with sepsis (*21*). Consistent with the substantial increase in myeloid cell counts, the proportion of myeloid-biased

multipotent progenitors ($MPP^{G/M}$) increased while lymphoid-biased ones (MPP^{Ly}) decreased (Fig. 1I). Compared to controls, $C5^{\Delta Vav}$ mice also had splenomegaly with increased numbers of neutrophils, macrophages, and dendritic cells (DCs), and reduced counts of natural killer cells (NKs) but no changes in B and T cells (Fig.1J, fig. S1I). Indicative of microbial dissemination, the spleens of $C5^{\Delta Vav}$ animals contained significant numbers of bacteria compared to the controls (Fig.1K). Importantly, intestinal and systemic inflammation were also observed in wild-type animals that received $C5^{\Delta Vav}$ bone marrow, demonstrating that the phenotype is due to loss of Arpc5 in hematopoietic cells (Fig.1L and fig. S1J).

The microbiota drives the inflammatory response in $C5^{\Delta Vav}$ animals.

At weaning there is a significant change in the intestinal microbiota that profoundly impacts mucosal homeostasis (*22*). To investigate the onset of pathologies induced by the absence of Arpc5, we assessed animals immediately after weaning (3 to 4 weeks old). We found there was no significant increase in feacal lipocalin-2 levels, mLN enlargement or intestinal pathology in 4wko $C5^{\Delta Vav}$ animals compared to control littermates (Fig.2A, fig. S2A, B). Nevertheless, the numbers of macrophages and DCs were elevated in 4wko $C5^{\Delta Vav}$ mLNs (fig. S2B), suggesting there is a progressive onset of inflammation after weaning. To explore whether local and systemic inflammation are triggered by commensal colonization after weaning, we treated 4wko $C5^{\Delta Vav}$ animals with an antibiotic cocktail prior to development of enteritis (Fig. 2B). This treatment prevented the development of enteritis, infiltration of macrophages and neutrophils into the ileum as well as subsequent systemic inflammation (Fig. 2C-E). Antibiotic treatment of $C5^{\Delta Vav}$ mice also suppressed splenomegaly (Fig. 2F fig.S2C), enlargement of mLNs and maintained normal cell populations in the bone marrow (Fig.2G, fig.S2D). Our observations demonstrate the onset of intestinal inflammation is progressive and driven by the microbiota.

Arpc5 is essential for intestinal homeostasis mediated by the innate immune system

We next sought to determine whether the phenotype seen in $C5^{\Delta Vav}$ mice was driven by a deficiency in innate and/or adaptive immune cells. To investigate the contribution of the adaptive immune system, we crossed $C5^{\Delta Vav}$ mice on to a *Rag*$^{-/-}$ background ($C5^{\Delta Vav/RagKO}$), which lack T and B cells.

$C5^{\Delta Vav/RagKO}$ mice had an even more pronounced phenotype with most animals reaching the humane endpoint around 6 weeks of life due to intestinal and systemic inflammation (Fig.3A and B and fig. S3A). Interestingly, in these $C5^{\Delta Vav/RagKO}$ mice the intestinal damage was now observed in the cecum (fig.S3A). Consistent with this, adoptive transfer of $C5^{\Delta Vav/RagKO}$ bone marrow into lethally irradiated wild-type mice also transferred the pathological phenotype, which was observed both in the cecum and small intestine (Fig.3C and D and fig. S3B and C). This confirms that the phenotypes seen in $C5^{\Delta Vav}$ mice are driven by deficiencies in innate immunity.

The current treatment for Wiskott-Aldrich Syndrome involves transplantation of hematopoietic stem/progenitor cells (*23, 24*). We decided to use a similar strategy, performing adoptive transfer of innate immune cells derived from *Rag*$^{-/-}$ bone marrow into 4wko $C5^{\Delta Vav}$ animals after myeloablation (Fig.3E). We found that $C5^{\Delta Vav}$ animals reconstituted with wild-type cells (C5-Rag^{KO}) had no signs of inflammation or the pathologies seen in $C5^{\Delta Vav}$ mice (Fig. 3F, fig. S3D and E). Mononuclear phagocytes (MNPs) play a key role in safeguarding intestinal homeostasis by clearing microbes that breach the ileal mucosa (*25-28*). Given this, we depleted MNPs in 4wko $C5^{\Delta Vav}$ animals with clodronate liposomes followed by adoptive transfer of $CD115^{+}$ MNPs from wildtype or $C5^{\Delta Vav}$ bone marrow (C5-$MØ^{WT}$ and C5-$MØ^{C5KO}$, Fig.3G). By 8-10 weeks, C5-$MØ^{C5KO}$ animals had higher faecal lipocalin-2 levels compared to C5-$MØ^{WT}$ mice (Fig.3H). The transplantation of wildtype $CD115^{+}$ MNPs also ameliorated the development of severe enteritis and systemic inflammation in $C5^{\Delta Vav}$ animals although minor inflammation was still present (Fig.3H, fig. S3F). Our observations emphasize the importance of innate immune cells and more specifically MNPs for the inflammatory phenotypes observed in the absence of Arpc5.

Arpc5 is required for efficient phagocytosis and bacterial killing

Arpc5 deficient bone marrow-derived macrophages (BMDMs) have striking differences in cell morphology, being less spread and more elongated than wild-type counterparts (Fig.4A, fig. S4A). These differences indicate that loss of Arpc5 impacts the organisations of the actin cytoskeleton as reported in other cell types (*18,29*). Our histological analysis, however, indicated that macrophages without Arpc5 readily infiltrate into the small intestine (Fig 1D), suggesting that defects in cell migration are not a major contributing factor in the phenotype of $C5^{\Delta Vav}$ mice.

Nevertheless, it was noticeable that BMDMs lacking Arpc5 had reduced levels of F-actin indicative of altered actin dynamics (Fig.4B, fig. S4B). It is well established that microbial internalization by phagocytes is actin dependent and defects in this process may contribute to inflammatory bowel disease (IBD) (*30, 31*). Consistent with this, we found that BMDMs lacking Arpc5 were less efficient in phagocytosing *E. coli* than controls and were defective in actin filament assembly (Fig.4B, C and fig. S4C, D). Live cell imaging of BMDMs expressing GFP-LifeAct revealed that the absence of Arpc5 resulted in a loss of actin rich ruffles that form around bacteria as they are phagocytosed (Fig 4D; movie 1). Furthermore, in contrast to wild-type BMDMs, the loss of Arpc5 also led to reduced bacterial killing as the number of intracellular bacteria remained constant (Fig.4E). Consistent with their defective bactericidal activity, infected BMDMs lacking Arpc5 were more prone to die (Fig.4F). Our in vitro analyses support the notion that Arpc5 deficient macrophages are defective in phagocytosing and killing microbes that breach the intestinal barrier.

Our analysis has uncovered that intestinal homeostasis depends on Arpc5, but not Arpc5l containing Arp2/3 complexes nucleating branched actin networks in innate immune cells. Moreover our data explain why patients lacking ARPC5 develop gastrointestinal complications, immunodeficiency and are prone to fatal sepsis. We propose that mutations in ARPC5 may contibute to IBD and should especially be considered in patients lacking damaging mutations in other candidate genes, such as ARPC1B and WAS (*32, 33*). Finally, our results suggest that bone marrow transplantation would revert the immunodeficiency of patients with ARPC5 loss of function mutations.

References and Notes

1.E. G. G. Sprenkeler, S. D. S. Webbers, T. W. Kuijpers, When Actin is Not Actin' Like It Should: A New Category of Distinct Primary Immunodeficiency Disorders. *J Innate Immun* **13**, 3-25 (2021).

2.E. Janssen, R. S. Geha, Primary immunodeficiencies caused by mutations in actin regulatory proteins. *Immunol Rev* **287**, 121-134 (2019).

3.A. J. Thrasher, S. O. Burns, WASP: a key immunological multitasker. *Nat Rev Immunol* **10**, 182-192 (2010).

4.L. M. Machesky, R. H. Insall, Scar1 and the related Wiskott-Aldrich syndrome protein, WASP, regulate the actin cytoskeleton through the Arp2/3 complex. *Curr Biol* **8**, 1347-1356 (1998).

5.L. M. Machesky *et al.*, Scar, a WASp-related protein, activates nucleation of actin filaments by the Arp2/3 complex. *Proc Natl Acad Sci U S A* **96**, 3739-3744 (1999).

6.S. Tur-Gracia, N. Martinez-Quiles, Emerging functions of cytoskeletal proteins in immune diseases. *J Cell Sci* **134**, (2021).

7.K. M. Glaser *et al.*, Arp2/3 complex and the pentose phosphate pathway regulate late phases of neutrophil swarming. *iScience* **27**, 108656 (2024).

8.E. D. Goley, M. D. Welch, The ARP2/3 complex: an actin nucleator comes of age. *Nat Rev Mol Cell Biol* **7**, 713-726 (2006).

9.A. M. Gautreau, F. E. Fregoso, G. Simanov, R. Dominguez, Nucleation, stabilization, and disassembly of branched actin networks. *Trends Cell Biol* **32**, 421-432 (2022).

10.J. V. Abella *et al.*, Isoform diversity in the Arp2/3 complex determines actin filament dynamics. *Nat Cell Biol* **18**, 76-86 (2016).

11.C. Galloni *et al.*, MICAL2 enhances branched actin network disassembly by oxidizing Arp3B-containing Arp2/3 complexes. *J Cell Biol* **220**, (2021).

12.L. Cao, S. Huang, A. Basant, M. Mladenov, M. Way, CK-666 and CK-869 differentially inhibit Arp2/3 iso-complexes. *EMBO Rep*, (2024).

13.T. W. Kuijpers *et al.*, Combined immunodeficiency with severe inflammation and allergy caused by ARPC1B deficiency. *J Allergy Clin Immunol* **140**, 273-277 e210 (2017).

14.W. H. Kahr *et al.*, Loss of the Arp2/3 complex component ARPC1B causes platelet abnormalities and predisposes to inflammatory disease. *Nat Commun* **8**, 14816 (2017).

15.L. O. Randzavola *et al.*, Loss of ARPC1B impairs cytotoxic T lymphocyte maintenance and cytolytic activity. *J Clin Invest* **129**, 5600-5614 (2019).

200 16.S. Volpi *et al.*, A combined immunodeficiency with severe infections, inflammation, and allergy caused by ARPC1B deficiency. *J Allergy Clin Immunol* **143**, 2296-2299 (2019).

17.C. J. Nunes-Santos *et al.*, Inherited ARPC5 mutations cause an actinopathy impairing cell motility and disrupting cytokine signaling. *Nat Commun* **14**, 3708 (2023).

18.E. Sindram *et al.*, ARPC5 deficiency leads to severe early-onset systemic inflammation and
205 mortality. *Dis Model Mech* **16**, (2023).

19.C. L. Abram, G. L. Roberge, Y. Hu, C. A. Lowell, Comparative analysis of the efficiency and specificity of myeloid-Cre deleting strains using ROSA-EYFP reporter mice. *J Immunol Methods* **408**, 89-100 (2014).

20.J. Stallhofer *et al.*, Lipocalin-2 Is a Disease Activity Marker in Inflammatory Bowel Disease
210 Regulated by IL-17A, IL-22, and TNF-alpha and Modulated by IL23R Genotype Status. *Inflamm Bowel Dis* **21**, 2327-2340 (2015).

21.X. Li *et al.*, Maladaptive innate immune training of myelopoiesis links inflammatory comorbidities. *Cell* **185**, 1709-1727 e1718 (2022).

22.Z. Al Nabhani *et al.*, A Weaning Reaction to Microbiota Is Required for Resistance to
215 Immunopathologies in the Adult. *Immunity* **50**, 1276-1288 e1275 (2019).

23.D. Moratto *et al.*, Long-term outcome and lineage-specific chimerism in 194 patients with Wiskott-Aldrich syndrome treated by hematopoietic cell transplantation in the period 1980-2009: an international collaborative study. *Blood* **118**, 1675-1684 (2011).

24.L. M. Burroughs *et al.*, Excellent outcomes following hematopoietic cell transplantation for
220 Wiskott-Aldrich syndrome: a PIDTC report. *Blood* **135**, 2094-2105 (2020).

25.N. Morita *et al.*, GPR31-dependent dendrite protrusion of intestinal CX3CR1(+) cells by bacterial metabolites. *Nature* **566**, 110-114 (2019).

26.M. Kim *et al.*, Critical Role for the Microbiota in CX(3)CR1(+) Intestinal Mononuclear Phagocyte Regulation of Intestinal T Cell Responses. *Immunity* **49**, 151-163 e155 (2018).

225 27.A. Mortha *et al.*, Microbiota-dependent crosstalk between macrophages and ILC3 promotes intestinal homeostasis. *Science* **343**, 1249288 (2014).

28.G. E. Diehl *et al.*, Microbiota restricts trafficking of bacteria to mesenteric lymph nodes by CX(3)CR1(hi) cells. *Nature* **494**, 116-120 (2013).

29.F. Fassler *et al.*, ArpC5 isoforms regulate Arp2/3 complex-dependent protrusion through
230 differential Ena/VASP positioning. *Sci Adv* **9**, eadd6495 (2023).

30.Y. R. Na, M. Stakenborg, S. H. Seok, G. Matteoli, Macrophages in intestinal inflammation and resolution: a potential therapeutic target in IBD. *Nat Rev Gastroenterol Hepatol* **16**, 531-543 (2019).

31.M. Krendel, N. C. Gauthier, Building the phagocytic cup on an actin scaffold. *Curr Opin Cell Biol* **77**, 102112 (2022).

32.S. Antala, B. Whitehead, H. Melin-Aldana, L. M. Bass, ARPC1B Mutation Manifesting as Recurrent Hematemesis With Metaplasia. *JPGN Rep* **2**, e095 (2021).

33.L. Jostins *et al.*, Host-microbe interactions have shaped the genetic architecture of inflammatory bowel disease. *Nature* **491**, 119-124 (2012).

34.J. Riedl *et al.*, Lifeact: a versatile marker to visualize F-actin. *Nat Methods* **5**, 605-607 (2008).

35.P. J. Koelink *et al.*, Development of Reliable, Valid and Responsive Scoring Systems for Endoscopy and Histology in Animal Models for Inflammatory Bowel Disease. *J Crohns Colitis* **12**, 794-803 (2018).

36.H. Aegerter *et al.*, Influenza-induced monocyte-derived alveolar macrophages confer prolonged antibacterial protection. *Nat Immunol* **21**, 145-157 (2020).

Acknowledgments:

We thank Patrick Costello, Chrysante Iliakis, and all staff in the Scientific Technology Platforms; Genetic Modification Service, Biological Research Facility, Experimental Histopathology, Cell Services and Flow Cytometry STPs for technical support. We also thank James Lee, Jeremy Carlton, Caetano Reis e Sousa, Andreas Wack, Maximiliano Gutierrez and Venizelos Papayannopoulos for reading the manuscript; Richard Treisman and Andreas Wack for sharing reagents. Experimental schematics in the paper were created using BioRender. For the purpose of open access, the authors have applied a CC BY public copyright licence to any author accepted manuscript version arising from this submission.

Funding: European Research Council (ERC) under the European Union's Horizon 2020 research and innovation programme grant agreement No 810207 (MW).

Francis Crick Institute, which receives its core funding from Cancer Research UK (CC2096) (MW) and (CC2016) (BS), the UK Medical Research Council (CC2096) (MW) and (CC2016) (BS), and the Wellcome Trust (CC2096) (MW) and (CC2016) (BS).

Author contributions:

Conceptualization: LRCV, MW, BS

Methodology: LRCV, SH, KS, NK, SB, MLW

Investigation: LRCV, SH, AS, SP

Visualization: LRCV, SH

Funding acquisition: MW

Project administration: MW, LRCV, SH, NK

Supervision: MW, BS

Writing – original draft: LRCV

Writing – review & editing: all authors.

Competing interests: Authors declare that they have no competing interests.

Data and materials availability: All data are available in the main text or the supplementary materials.

Supplementary Materials

Materials and Methods

Mice

In the present study we utilized sex and age-matched (4-15 weeks old) C57Bl/6 mice, from both genders, bred at the Francis Crick Institute (2019-2024) under pathogen-free conditions. Mice were genotyped before weaning by Transnetyx and randomly assigned to treatment groups and blinding strategies applied when possible. For adoptive transplantation, both *Ptprc*^{a} (CD45.1) and *Ptprc*^{b} (CD45.2) were used. The genetically modified animals *Arpc5*$^{\text{Cre-Vav1}}$, *Rag1*$^{-/-}$, *Rag1*$^{-/-}$/*Arpc5*$^{\text{Cre-Vav1}}$, C57Bl/6$^{\text{LifeAct-GFP}}$ and *Arpc5*$^{\text{Cre-Vav1}}$/ $^{\text{LifeAct-GFP}}$ (*34*) were used in the present study. All in vivo experiments were performed following the Act 1986 for animal scientific procedures

after the approval by the review board of The Francis Crick Institute and the Home Office (United Kingdom) under project licence PP0792028.

The conditional Arpc5 knockout mouse model has been previously reported (*18*). The Arpc5l conditional knockout was generated by the Crick Genetic Modification Service using a similar CRISPR-Cas9 approach in embryonic stem cells (ESCs). Briefly, the gRNA-1: 5'-CTCTGGATAGAGACAACAGA-3' and gRNA-2: 5'-CATCCCCGATAGAGCTACAT-3' were used to introduce the 5′ and 3′ loxP sites flanking exon 2 of the Arpc5l gene. Deletion of exon 2 results in a frameshift and an exogenous stop codon within exon 3. The Cas9-gRNA-Puro plasmids were generated by inserting the CRISPR-Cas9 target sequences into PX459 plasmid (Addgene plasmid #48139). The pMA donor plasmid contained a synthesized 1049 bp fragment corresponding to exon 2 flanked by loxP sites and 1 kb flanking homology arms (GeneArt, Thermo Fisher Scientific). Sequence-verified Cas9-gRNA-Puro plasmids and pMA donor plasmid were co-transfected into in-house C57BL6/N 6.0 ESC using Lipofectamine 2000 (Thermo Fisher Scientific) and selected with puromycin. Integration of 5′ and 3′ loxP sites were identified by reverse transcription quantitative polymerase chain reaction (RT-PCR) assays on genomic DNA using gene-specific probes designed by Transnetyx and the integrity of the loxP integrations was confirmed by PCR amplicons sequencing. ESC clones were microinjected into C57BL/6J mice blastocysts [B6(Cg)-Tyrc-2J/J; strain #000058, The Jackson Laboratory) and then transplanted into the uteri of pseudo-pregnant CD1 females. The resulting chimeras were crossed to albino C57BL/6J, and their offspring screened for the integration of the loxP sites by amplicon sequencing. Heterozygous floxed offspring were validated by sequencing and two founder strains maintained on a C57BL/6J background.

Disease activity index and histology

To assess the enteritis disease activity index (DAI), we followed a modified scoring system as described previously (*35*). Briefly, mice were evaluated using signs of clinical disease including weight loss, faecal consistency and presence of blood, and lack of movement. All parameters were assessed using a semi-quantitative grading scheme as follows: 0, no disease; 1, mild; 2, moderate; 3, marked; 4, severe.

Intestines ('Swiss rolls') and other organs were collected, fixed for 48h in 10% neutral buffered formalin which was subsequently replaced with 70% ethanol, embedded in paraffin wax and sectioned at 4µm. Sections were stained with H&E then microscopically examined by two certified veterinary pathologists blinded to the grouping and genotypes. Histopathological analyses considered the presence and extent of tissue inflammation and epithelial injury. All parameters were assessed in a semi-quantitative grading scheme for severity as follows: 0, no lesion; 1, minimal change; 2, mild change; 3, moderate change; 4, marked change; 5, severe.

Quantification of total leukocytes, macrophages and neutrophils immunohistochemistry was performed using anti-CD45, anti-F4/80 or anti-2B10, respectively, conjugated with a horseradish peroxidase (HRP) secondary antibody and using DAB chromogen. The slides were scanned with a Zeiss Axio Scan.Z1 annotated and processed with QuPath software (v0.4.3). To account for the prevalence of target cells, 10 different random regions (750µm^2) were analyzed for positive labelling using hematoxylin as counterstaining. The values are presented as prevalence (%) of the Target cell/ Total cells.

Irradiated chimeras

CD45.1$^+$ wild-type recipient mice at 10-13 weeks old were lethally irradiated with ^{137}Cs-irradiated 2 × 6 Gy with a 3-hour interval. For reconstitution, 10 x 10^6 bone marrow cells from donors (CD45.2$^+$, as indicated in figures) were injected intravenously via tail vein into the recipients (CD45.1$^+$). Bone marrow cells were collected from femur and tibia of donor mice and washed through a 70µm cell strainer. At 5-10 weeks later, the animals were euthanized, samples collected, and engraftment verified by flow cytometry. Distinction between donor and recipient cells was assessed by CD45.1 or CD45.2 expression.

Antibiotic treatment

Four week old *Arpc5*$^{\text{Cre-Vav1}}$ (C5$^{\Delta\text{Vav}}$) mice were treated continuously for 4 weeks in the drinking water with an antibiotic cocktail (Atbx) consisting of ampicilin (1mg/mL), gentamicin (1mg/mL),

345 metronidazole (1mg/mL), neomycin (1mg/mL), vancomycin (500µg/mL) and sucralose-based artificial sweetener (100mg/mL, The Pantry) or artificial sweetener only (vehicle). Mice were euthanized, and samples collected after treatment.

Busulfan chimeras

350 Four week old *Arpc5*$^{\text{Cre-Vav1}}$ (C5$^{\Delta\text{Vav}}$) mice were treated with 10mg/kg Busilvex (busulfan-Pierre Fabre) intraperitoneally for 2 consecutive days with a 24h interval. Donor bone marrow cells (10 x 10^6) in 100µl PBS were injected intravenously into the tail vein, 24h after the second busulfan dose (*36*). Bone marrow cells were collected from femur and tibia of donor mice and washed through a 70µm cell strainer. After adoptive cell transfer, animals were kept for 8-10 weeks before 355 euthanasia and sample collection. CD45.1 and CD45.2 expression were used to differentiate between donor and recipient cells in transplanted animals.

In vivo macrophage depletion and adoptive cell transfer

Four week old *Arpc5*$^{\text{Cre-Vav1}}$ (C5$^{\Delta\text{Vav}}$) mice received intraperitoneal injection of 5µl/g 360 clodronate_SUV_PEG liposomes (CP-SUV-P-005-005-Liposoma) and 48h later were adoptively transferred with 3 x 10^6 CD115$^+$ isolated from wild-type or C5$^{\Delta\text{Vav}}$ mice bone marrows following the manufacturer's instructions (Miltenyi Biotec, #130-096-354).

Immunoblot and Enzyme-linked immunosorbent assay (ELISA)

365 Cells and tissue extracts were lysed for 15 min on ice in RIPA buffer supplemented with protease and phosphatase inhibitors (Roche, catalogue number). Protein extracts were quantified, and similar amounts of total cell lysate separated by SDS-PAGE, followed by immunoblot analysis.

Antibodies used for immunoblots: Arp3 (Sigma-Aldrich, A5979), ArpC1A (Atlas antibodies, HPA004334), ArpC1B (Bethyl Lab, A302-781A), ArpC2 (Abcam, ab133315), ArpC5 (Synaptic 370 Systems, 305011), ArpC5L (Proteintech, 22025-a-AP), β -actin (Abcam, ab179467), anti-mouse IgG-IRDye® 800CW (LI-COR Biosciences, 926-32210) and anti-rabbit IgG-IRDye® 680RD (LI-COR Biosciences, 926-68071).

For LPCN-2 assessment, fresh faeces pellets were obtained and weighed prior to maceration in
375 300µl of PBS 0.1% triton X100 (Sigma) followed by ELISA detection. The levels of Lipocalin-2 (LPCN-2, DY1857-05) and C-reactive protein (CRP, MCRP00) were detected following the manufacturer's instructions (R&D Systems).

Splenic Colony forming units (CFU)

380 Mouse spleens were dissociated in 500µl PBS 0.2% NP40 (Merck-492016) and centrifuged at 400x*g* for 3 min at room temperature to pellet debris. 100µl of the supernatant was plated on LB agar, incubated at 37ºC for 24h and CFU determined.

Flow cytometry

385 Single cell suspension was preincubated with viability dye and FcgRIII/II (Fc block) before 30 min of incubation with fluorochrome-labelled antibodies or phalloidin. The stained cells were analyzed using BD LSR Fortessa cell analyser (BD Biosciences) and interpreted using Flowjo software (v.10.6.2). For intracellular staining cells were fixed and permeabilized using the Foxp3/Transcription Factor Staining Buffer Set (00-5523-00 ThermoFisher Scientific). FACs
390 buffer (Thermo Fisher Scientific, 00-4222-26), Live/Dead^{TM} Fixable Near-IR Dead Cell Stain Kit (Thermo Fisher Scientific, L10119).

The following antibodies (supplied by Biolegend or the indicated company) were used in flow cytometry: CD16/32 Fcx (101320), B220-FITC (103205), B220-PerCP (103234), B220-APC
395 (103212), CD2-FITC (100105), CD3-BV711 (100241), CD3-BUV395 (BD, 563565), CD4-BV605 (100548), CD4-BV711 (100557), CD8a-BV650 (100742), CD8a-BV737 (BD, 612759), CD8a-PE/Cy7 (100722), CD8b-BV786 (BD, 740952), CD11b-BV421 (101236), CD11b-BV711 (101242), CD11b-BV785 (101243), CD11c-AF488 (117311), CD11c-BV605 (117334), CD11c-BUV563 (BD, 749040), CD19-BV711 (115555), CD16/32-BV711 (101337), CD19-APC/Cy7
400 (BD, 557655), CD45-APC (103112), CD45-BUV395 (BD, 564279), CD45.1-AF700 (110724), CD45.2-BV785 (109839), CD48-PE (103406), CD64-PeCy7 (139314), CD71-PE (113807),

CD103-AF488 (121408), CD103-BV605 (BD, 740355), CD117-APC (BD, 553356), CD135-BV421 (BD, 562898), CD150-BV605 (115927), F4/80 (Invitrogen, 17-4801-82), Foxp3-PE (126404), Foxp3-AF700 (126422), Gr-1-FITC (108406), Gr-1-BV711 (108443), I-A/I-E-AF488 (107616), I-A/I-E-AF700 (107622), Ly6C-BV785 (128041), Ly6C-APC (128016), Ly6G-FITC (BD, 551460), NK1.1-BV711(108745), NK1.1-PE (BD, 557391), TCRab-BV421 (109230), TCRgd-APC (118116), TCRab-PE (eBioscience, 12-5961-82), Ter119-FITC (116206), Sca-1-PE/Cy7 (Invitrogen, 25-5981-82), AntiDNAse-I (Invitrogen, D12371).

Differentiation of bone marrow derived macrophages

Bone marrow was collected from the tibia and femur of mice and differentiated in vitro for 7 days in RPMI (Gibco R8758) supplemeted with 10% fetal bovine serum (Gibco, 10270-106), 10% L929 conditioned medium (Crick Cell services STP), L-glutamine (Stem Cell technologies, 07100), penicilin/streptramycin (Gibco, 15140-122), non-essential amino acids (Gibco, 11140-035), and sodium pyruvate (Gibco, 11360-039) to obtain bone marrow derived macrophages (BMDM).

Phagocytosis, bacterial killing and cytotoxicity assays in BMDM

To assess bacterial phagocytosis, adhered BMDMs (5 x 10^5) were incubated with FITC-Heat-killed (HK) *E.coli* (60µg/mL-E2861-Invitrogen) or pHrodo *E.coli* (1µg/mL-P35366-Invitrogen) for up to 120 min at 37ºC, 5% CO_2. Negative controls were incubated at 4ºC during the same period. Bacterial uptake was assessed by flow cytometry using the phagocytosis index calculation as follows: [(MFI x % positive cells at 37ºC) – (MFI x % positive cells at 4ºC)].

For bacterial killing (3x10^5 BMDMs in 12 well plates) and cytotoxicity assays (10^5 BMDMs in 96 well plate) adherent BMDM were incubated with phase *E. coli* K-12 (NCTC_10538) mid-log at MOI 5, 10 or 50. The bacteria concentration was assessed using OD_{600}. The BMDM killing capacity was assessed by microscopy. Ten random fields of view were imaged on a Zeiss Axio Observer spinning-disk microscope equipped with a Plan Achromat 63×/1.4 Ph3 M27 oil lens, an Evolve 512 camera, and a Yokagawa CSUX spinning disk. The microscope was controlled by the SlideBook software (3i Intelligent Imaging Innovations). Images were analyzed using FIJI and internalized bacteria were detected using anti-E coli (abcam, ab137967). Microscopy secondary

antibodies (catalogue number) and DAPI (catalogue number). Calculations were obtained as follows: [(internalized bacteria at T0) – (internalized bacteria at Time X)].

435 The BMDMs cytotoxicity was assessed using the CyQUANT^{Tm}LDH Cytotoxicity assay following the manufacturer's instructions (Thermo Fisher Scientific, C20300). For G-actin or F-actin detection, BMDMs ($5x10^5$ in non-adherent 6 well plates) were incubated with E. coli K-12 (MOI 50) for 15 min or vehicle. 30 min pre-treatment with 10µM Cytochalasin D (Merck, 250255) was performed when indicated. After treatment cells were permeabilized using the
440 Foxp3/Transcription Factor Staining Buffer Set (00-5523-00 ThermoFisher Scientific) and stained with antiDNAse-I Alexa Fluor 488 (Invitrogen, D12371) or Alexa Fluor 568-phalloidin (Molecular Probes), respectively.

Morphological and live cell imaging of BMDM

445 BMDM$^{LifeAct-GFP}$ derived from C5^{HetVav} or C5$^{\Delta Vav}$ murine bone marrow were seeded on fibronectin coated 35 mm Matek dish at $5x10^4$ cells/well and incubated overnight at 37°C with 5% CO_2. Cells were imaged as described above. Data for 10-12 cells per sample were segmented using ilastik and segmented images were then analyzed using FIJI. For live cell imaging the cells were seeded on fibronectin coated ibidi 4-well glass-bottom µ-slide at $4x10^4$ cells/well and incubated overnight
450 at 37°C with 5% CO_2. pHrodo™ Deep Red E. coli BioParticles™ Conjugate (Thermo Fisher) was prepared according to manufacturer's instructions. Prior to imaging, 5 µL of pHrodo™ Deep Red E. coli was added into each well. The imaging chamber was maintained at 37°C. Cells were imaged every 500 ms for 5 minutes using a Zeiss Axio Observer microscope equipped with a Plan Achromat 100x/1.46 oil lens, an Evolve 512 camera, and a Yokagawa CSUX spinning disk. The
455 microscope was controlled by the SlideBook software (3i Intelligent Imaging Innovations).

Statistical analysis

Data are shown as the mean ± S.E.M. Sample sizes were established prior to experimental approach with help of the experimental design assistant of NC3Rs to achieve statistical power
460 while minimizing animal use. To test normality or lognormality we applied D'Agostino & Pearson

test. All statistical comparisons were performed using Prism 10 (GraphPad) with specific statistical test applied as stated in the figure legends. Statistical significance was considered as $P<0.05$.

465 **Legends**

Figure 1. Arpc5 loss in immune cells leads to intestinal damage and systemic inflammation. **(A)** The level of Arpc5 and Arpc5l in $C5^{fl/fl}$, $C5^{HetVav}$ or $C5^{\Delta Vav}$ bone marrow extracts. (**B**) Lipocalin-2 (LPCN-2) faecal levels in the indicated mice. (**C**) H&E images of intestines (left) together with quantification of the histopathology score (middle) and disease activity index (DAI)
470 (right). (**D**) Immunohistochemistry reveals the increased prevalence of macrophages (top) and neutrophils (bottom) in ileal sections in mice lacking Arpc5. (**E**) Loss of Arpc5 increases the size and cell counts of Mesenteric lymph nodes (mLNs) but not the inguinal lymph node (iLN). (**F**). Mice lacking Arpc5 have increased levels C-reactive protein (CRP) as well as phagocytes in their blood. (**G**) Quantification of the counts of neutrophils (NØs) and $Ly6C^{hi/lo}$ monocytes (MØs) in
475 peripheral blood of the indicated mice. **(H)** Representative images together with the quantification of the counts of erythroid lineage and immature neutrophil (NØ) in the bone marrow of the indicated mice. (**I**) Quantification of the % of multipotent progenitors (MPP) among the $lineage^{-}$ $Sca1^{+}c\text{-}Kit^{+}$ (LSK) cells. MPP-Ly: lymphoid-biased MPPs; MPP-G/M: myeloid-biased MPPs; MPP-MkE: megakaryocyte and erythroid-biased MPPs; MPP: unbiased MPPs. (**J**) Representative
480 image and weight of spleen in the indicated mice. (**K**) Bacterial colony forming units (CFU) in $C5^{HetVav}$ or $C5^{\Delta Vav}$ mice spleens. (**L**) Schematic of the bone marrow transplantation protocol: CD45.1_wild type mice were lethally irradiated and reconstituted with either CD45.2_controls (WT-Control) or CD45.2_$C5^{\Delta Vav}$ (WT-$C5^{\Delta Vav}$) bone marrow. H&E image of intestines of animals which received wild-type (WT-control) or $C5^{\Delta Vav}$ (WT-$C5^{\Delta Vav}$) bone marrow transplantation.
485 Animals assessed in this figure were 8-15 week old mice n=7 of two independent experiments. Data shown as means ± SEM of at least three independent experiments, n=8. Statistical analysis was performed using Kruskal-Wallis test in **B**, Mann-Whitney test in **C**, **E, F**, **H, J, K, L,** one-way ANOVA in **G** and **I,** or multiple Mann-Whitney test in **D**. Significant *p* values are indicated

on the graphs. $C5^{fl/fl}$ ($arpc5^{fl/fl}$), $C5^{HetVav}$ ($arpc5^{HetVav}$) and $C5^{\Delta Vav}$ ($arpc5^{\Delta Vav}$). ns = not significant. * = p-value < 0.05. ** = p-value < 0.01. *** = p-value < 0.001 and **** = p-value < 0.0001.

Figure 2. The intestinal dyshomeostasis upon Arpc5 loss is microbiota dependent. (**A**) Lipocalin-2 (LPCN-2) faecal levels (left), quantification of the histopathology score (middle) and H&E image of the ileum of 4 weeks old (4wko) $C5^{HetVav}$ or 4 and 8wko $C5^{\Delta Vav}$ animals (right). (**B**) Experimental scheme of antibiotic treatment; 4wko animals were treated with antibiotic cocktail (Atbx) or vehicle (Veh) for 4 weeks and then sampled for analysis. (**C**) Quantification of LPCN-2 levels in faeces (left), and histopathology score (middle) together with H&E image of the ileum in the indicated mice (right). (**D**) Representative immunohistochemistry images and quantification showing Atbx treatment reduces macrophages (top) and neutrophils (bottom) presence in ileal sections in $C5^{\Delta Vav}$ mice. (**E**) Levels of C-reactive protein (CRP) in the blood of animals with and without antibiotic treatment. (**F**) Representative images and weight of spleens animals with and without antibiotics. (**G**) Representative image together with the quantification of numbers of immature neutrophil (NØ) in the bone marrow of mice with and without antibiotic treatment. Data shown as means ± SEM of at least three independent experiments, n=7. Statistical analysis was performed using Kruskal-Wallis tests in **A**, **C**, **E**, **F** and **G,** or Mann-Whitney test in **D**. Significant *p* values are indicated on the graphs. Controls used were $arpc5^{HetVav}$ and $C5^{\Delta Vav}$ ($arpc5^{\Delta Vav}$). ns = not significant. * = p-value < 0.05. ** = p-value < 0.01. *** = p-value < 0.001 and **** = p-value < 0.0001.

Figure 3. Arpc5 is essential for effective innate immunity. (**A**) Levels of C-reactive protein (CRP) in the serum and (**B**) quantification of disease activity index (DAI including values also shown in Fig.1C, left) and histopathology score together with representative H&E images of cecum of $control^{RagKO}$ or $C5^{\Delta VavRagKO}$ mice (right). (**C**) Schematic of the bone marrow transplantation protocol: CD45.1_wildtype mice were subjected to lethal irradiation and reconstituted with either CD45.2_$control^{RagKO}$ (WT-CT^{RagKO}) or CD45.2_$C5^{\Delta VavRagKO}$ (WT-$C5^{\Delta VavRagKO}$) bone marrow. (**D**) Levels of CRP(left) and quantification of the histopathology score in irradiated mice together with representative H&E images of ileum (right). (**E**) Scheme for adoptive cell transfer after busulfan treatment: 4 weeks old $C5^{\Delta Vav}$ mice were treated with busulfan and injected with either WT (C5-$Rag^{-/-}$) or $C5^{\Delta Vav}$ (C5-$C5^{\Delta Vav}$) innate cells. (**F**) Lipocalin-2 (LPCN-2) faecal levels (left) and quantification of the histopathology score

together with representative H&E images of the ileum of busulfan-treated mice (right). (**G**) Clodronate liposome treatment scheme: clodronate liposomes were injected into 4 weeks old animals followed by wild-type (MØ^{WT}) or C5$^{\Delta Vav}$ (MØ^{KO}) CD115^{+} cell transplantation n=5 of two independent experiments. (**H**) LPCN-2 faecal levels (left) and quantification of the histopathology score together with representative H&E images of the ileum (right) of indicated animals after clodronate depletion followed by adoptive cell transfer. Data shown as means ± SEM of at least three independent experiments, n=8 except as indicated in (H). Statistical analysis was performed using Mann-Whitney test in **A**, **B** (right), **D, F** and **H** and multiple Mann-Whitney test in **B** (left). Significant *p* values are indicated on the graphs. Controls used were Arpc5$^{HetVav/RagKO}$. C5$^{\Delta VavRagKO}$ (Arpc5$^{\Delta Vav/RagKO}$). Clo = clodronate liposomes. ns = not significant. * = p-value < 0.05. ** = p-value < 0.01. *** = p-value < 0.001 and **** = p-value < 0.0001.

Figure 4. ArpC5-mediated actin remodeling is key to macrophage biology. (A) Representative images of the actin cytosksleton in bone marrow derived macrophages (BMDMs) with or without Arpc5 together with quantification of their cell area and circularity. (**B**) Ratio of F-actin/G-actin in resting or *E.coli*-activated BMDMs incubated with vehicle or pretreated with 10µM Cytochalasin D for 30min. (**C**) Quantification of *E. coli* phrodo particle uptake by BMDMs. (**D**) Representative images showing the actin cytoskeleton dynamics (Cyan) visualized with GFP-Lifeact in wildtype and Arpc5$^{-/-}$ BMDMs during *E. coli* (Red) phagocytosis. The time in each panel is seconds. (**E**) The quantification of the percentage of internalized bacteria by BMDMs. (**F**) *E. coli* infection induced BMDM cell death. Data shown as means ± SEM of at least three independent experiments. Statistical analysis was performed using unpaired *t* test in **A** or two-way analysis of variance (ANOVA) in other graphs. Significant *p* values are indicated on the graphs. C5$^{+/+}$ = Arpc5$^{+/+}$, C5$^{-/-}$ = Arpc5$^{-/-}$. Scale bars = 10µm. ns = not significant. * = p-value < 0.05. ** = p-value < 0.01. and **** = p-value < 0.0001.

Suppl.1. (A) Arpc5 deletion strategy using Vav1-iCre. (**B**) Weight change (g) of C5$^{fl/fl}$, C5^{HetVav} or C5$^{\Delta Vav}$ mice over 15 weeks. (**C**) Representative H&E images of the ileum rolls. (**D**) Quantification of the histopathology score of intestines of indicated 8-15 wks old mice. (**E**) Cell numbers of mesenteric lymph nodes (mLNs) B and T cells, CD4^{+} and CD8^{+}, macrophages (MØs), neutrophils (NØs) and dendritic cells (DCs) in the indicated mice. (**F**) The levels of Arpc5 and Arpc5l in C5L^{HetVav} or C5L$^{\Delta Vav}$ bone marrow extracts, actin is a loading control. (**G**)

Representative H&E images of ileum rolls and Lipocalin-2 (LPCN-2) faecal levels in the indicated mice. (**H**) Cell numbers of B, CD4+, CD8$^+$ and NK lymphocytes in the blood of indicated mice. (**I**). NØs, MØs, DCs, B lymphocytes, CD4$^+$, CD8$^+$ and NK cells numbers in the spleen of C5^{HetVav} or C5$^{\Delta Vav}$ mice. (**J**) Quantification of the levels of C-reactive protein (CRP) in the serum and LPCN-2 in the faeces of indicated animals after bone marrow transplantation. (L) Representative H&E images of ileum rolls of indicated animals after bone marrow transplantation. (M) Spleen weight (right) in indicated animals after bone marrow transplantation. Data shown as means ± SEM of at least three independent experiments, n=8. Statistical analysis was performed using Kruskal-Wallis test in **B**, **D** and **I** one-way analysis of variance (ANOVA) in **E** and **G,** Mann-Whitney test in **H** and **K** and significant *p* values are indicated on the graphs. C5$^{fl/fl}$ (arpc5$^{fl/fl}$), C5^{HetVav} (arpc5^{HetVav}), C5$^{\Delta Vav}$ (arpc5$^{\Delta Vav}$) and C5L$^{\Delta Vav}$ (arpc5l$^{\Delta Vav}$). ns = not significant. * = p-value < 0.05. ** = p-value < 0.01. *** = p-value < 0.001 and **** = p-value < 0.0001.

Suppl.2. (**A**) Representative H&E image of ileum rolls of 4 weeks old C5^{HetVav} or C5$^{\Delta Vav}$ mice. (**B**) Total cell numbers in mLNs of 4 and 8 weeks old (left) together with the cell counts of B, T and CD4$^+$ or CD8$^+$ lymphocytes (middle), neutrophils (NØs), macrophages (MØs) or dendritic cells (DCs) (right) in mLNs from 4 wko C5^{HetVav} or C5$^{\Delta Vav}$ mice. (**C**) Splenic B, T and NK lymphocytes (left), NØs, MØs and DCs (right) cell counts in the indicated mice after antibiotic treatment. (**D**) mLNs total cell counts (left), together with NØs and MØs (middle), B and T lymphocytes (right) cell numbers from mLNs of mice treated with antibiotic. Data shown as means ± SEM of at least three independent experiments, n=7. Statistical analysis was performed using Kruskal-Wallis test and significant *p* values are indicated on the graphs. Controls used were C5^{HetVav} (arpc5^{HetVav}), C5$^{\Delta Vav}$ (arpc5$^{\Delta Vav}$). ns = not significant. * = p-value < 0.05. ** = p-value < 0.01. *** = p-value < 0.001 and **** = p-value < 0.0001.

Suppl.3. (**A**) Spleen weight (left) and representative H&E images of cecum of control^{RagKO} or C5$^{\Delta VavRagKO}$ mice (right). (**B**) Representative Facs plots (left) and quantification of CD45.1$^+$ or CD45.2$^+$ of mice after bone marrow transplantation (right). (**C**) Spleen weight (left) and faecal lipocalin-2 (LPCN-2) levels (right) in indicated mice after bone marrow transplantation. (**D**) Representative image of H&E images of ileum rolls. (**E**) Quantification of the levels of serum C-reactive protein (CRP), spleen weight, mLNs cell counts and immature neutrophils (NØs) counts in the bone marrow of indicated animals after busulfan adoptive transfer. (**F**) CRP levels in the

serum of indicated animals after clodronate depletion followed by adoptive cell transfer n=5 of two independent experiments. Data shown as means ± SEM of at least three independent experiments, n=8. Statistical analysis was performed using Mann-Whitney test in **A**, **C** and **F** Kruskal-Wallis test in **E**. Significant *p* values are indicated on the graphs. Controls used were arpc5^{HetVav} and C5$^{\Delta Vav}$ (arpc5$^{\Delta Vav}$). ns = not significant. * = p-value < 0.05. ** = p-value < 0.01. *** = p-value < 0.001 and **** = p-value < 0.0001.

Suppl.4. (**A**) Representative Facs plot and measurements of side scatter area (SSC-A) or forward scatter area (FSC-A) of indicated bone marrow derived macrophages (BMDMs). (**B**) Facs histograms of G-actin or F-actin in unstimulated BMDMs. (**C**) Quantification of *E coli*-FITC uptake by C5$^{+/+}$ or C5$^{-/-}$ BMDMs in the indicated timepoints. (**D**) Representative F-actin Facs histograms of *E.coli*-activated BMDMs. Data shown as means ± SEM of a representative of at least three independent experiments. Statistical analysis was performed using one-way analysis of variance (ANOVA) in **A** and two-way ANOVA in **C**. Significant *p* values are indicated on the graphs. C5$^{+/+}$ = Arpc5$^{+/+}$, C5$^{-/-}$ = Arpc5$^{-/-}$. *** = p-value < 0.001 and **** = p-value < 0.0001.

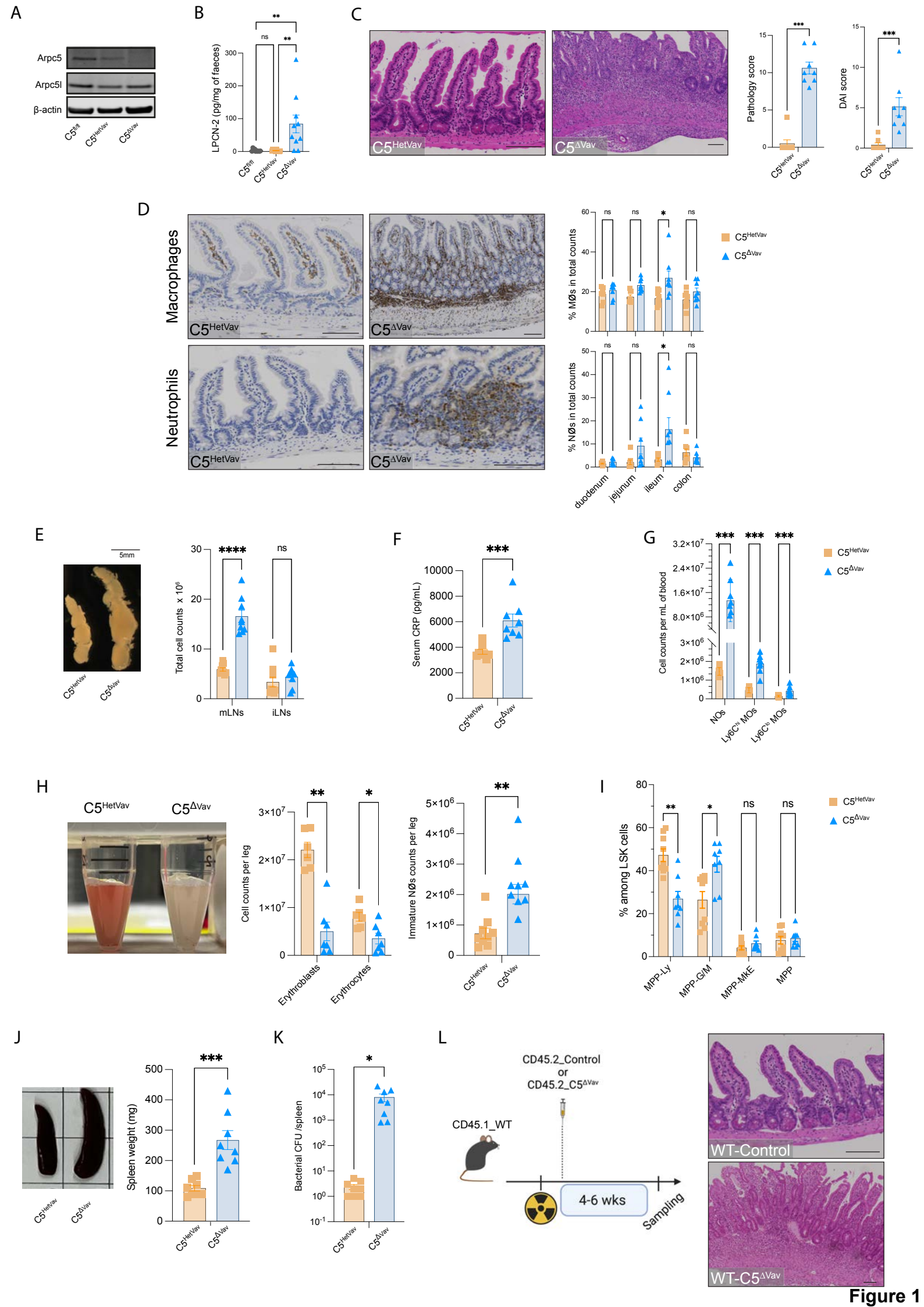
A
Arpc5
Arpc5l
β-actin
C5fl/fl
C5HetVav
C5ΔVav
B
LPCN-2 (pg/mg of faeces)
ns
**
C
C5HetVav
C5ΔVav
Pathology score
DAI score
***
D
Macrophages
Neutrophils
% MØs in total counts
% NØs in total counts
ns
*
duodenum
jejunum
ileum
colon
E
5mm
Total cell counts x 10^6
****
mLNs
iLNs
F
Serum CRP (pg/mL)
G
Cell counts per mL of blood
NOs
Ly6Chi MOs
Ly6Clo MOs
H
Cell counts per leg
Erythroblasts
Erythrocytes
Immature NØs counts per leg
I
% among LSK cells
MPP-Ly
MPP-Gl/M
MPP-MkE
MPP
J
Spleen weight (mg)
K
Bacterial CFU /spleen
L
CD45.2_Control
or
CD45.2_C5ΔVav
CD45.1_WT
4-6 wks
Sampling
WT-Control
WT-C5ΔVav

Figure 1

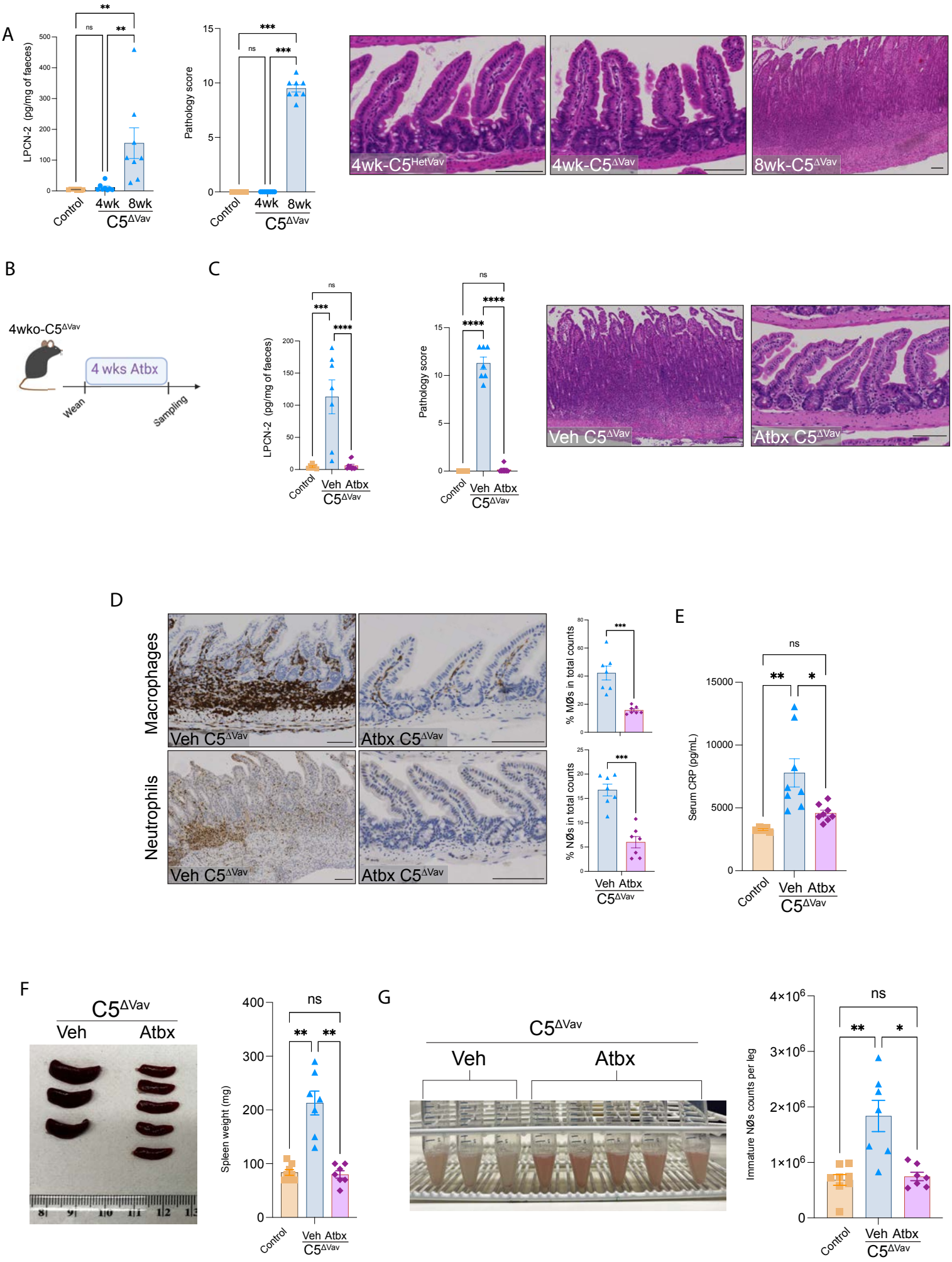
A
LPCN-2 (pg/mg of faeces)
Control
4wk
8wk
C5ΔVav
Pathology score
4wk-C5HetVav
4wk-C5ΔVav
8wk-C5ΔVav
B
4wko-C5ΔVav
4 wks Atbx
Wean
Sampling
C
LPCN-2 (pg/mg of faeces)
Pathology score
Veh
Atbx
Veh C5ΔVav
Atbx C5ΔVav
D
Macrophages
Neutrophils
% MØs in total counts
% NØs in total counts
E
Serum CRP (pg/mL)
F
C5ΔVav
Veh
Atbx
Spleen weight (mg)
G
Immature NØs counts per leg

Figure 2

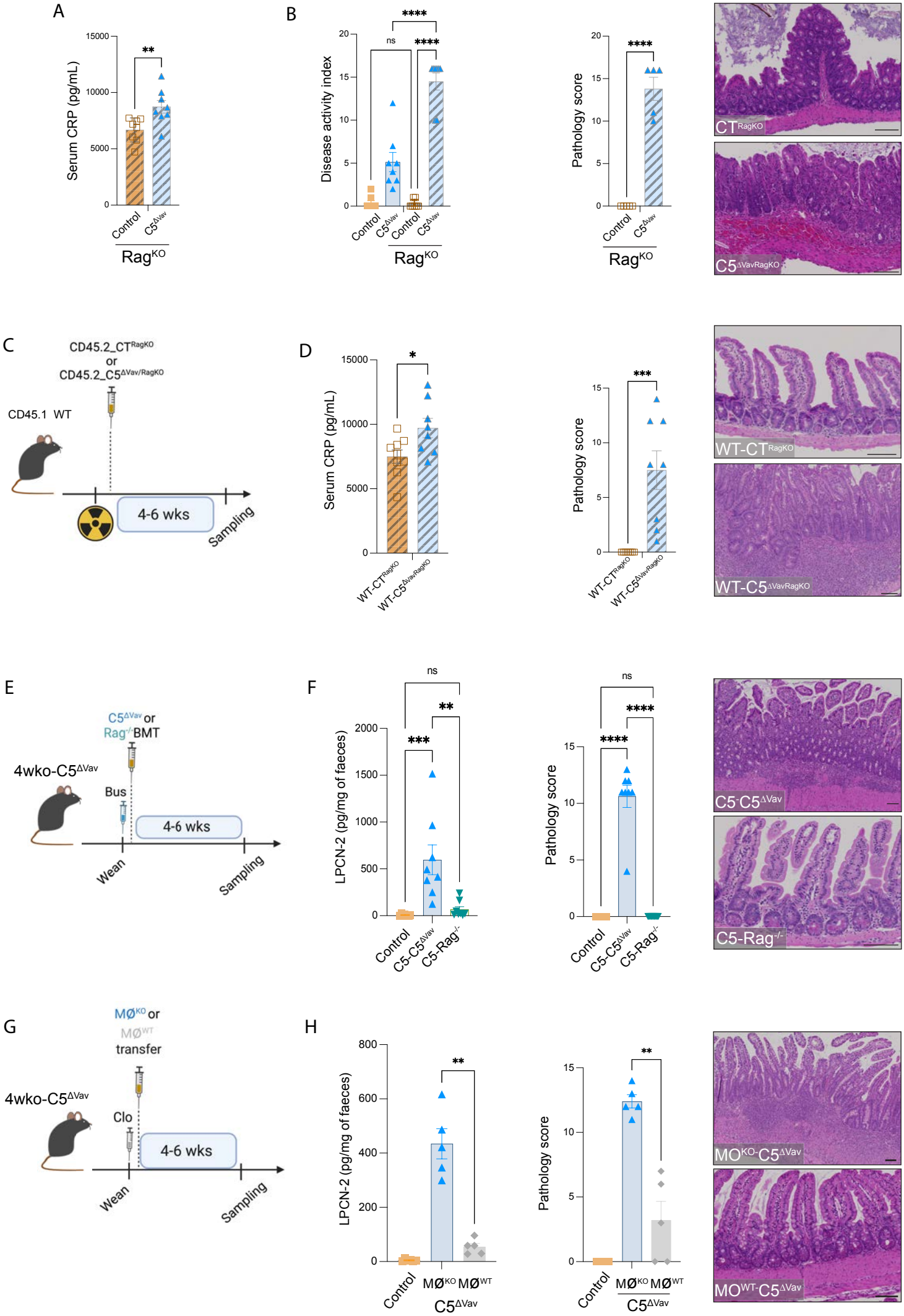
A
Serum CRP (pg/mL)
15000
10000
5000
0
**
Control
C5ΔVav
RagKO
B
Disease activity index
20
15
10
5
0
****
ns
****
Control
C5ΔVav
Control
C5ΔVav
RagKO
Pathology score
20
15
10
5
0
****
Control
C5ΔVav
RagKO
CTRagKO
C5ΔVavRagKO
C
CD45.2_CTRagKO
or
CD45.2_C5ΔVav/RagKO
CD45.1 WT
4-6 wks
Sampling
D
Serum CRP (pg/mL)
15000
10000
5000
0
*
WT-CTRagKO
WT-C5ΔVavRagKO
Pathology score
15
10
5
0
***
WT-CTRagKO
WT-C5ΔVavRagKO
WT-CTRagKO
WT-C5ΔVavRagKO
E
C5ΔVav or
Rag-/- BMT
4wko-C5ΔVav
Bus
4-6 wks
Wean
Sampling
F
LPCN-2 (pg/mg of faeces)
2000
1500
1000
500
0
ns
**
***
Control
C5-C5ΔVav
C5-Rag-/-
Pathology score
15
10
5
0
ns
****
****
Control
C5-C5ΔVav
C5-Rag-/-
C5-C5ΔVav
C5-Rag-/-
G
MØKO or
MØWT
transfer
4wko-C5ΔVav
Clo
4-6 wks
Wean
Sampling
H
LPCN-2 (pg/mg of faeces)
800
600
400
200
0
**
Control
MØKO MØWT
C5ΔVav
Pathology score
15
10
5
0
**
Control
MØKO MØWT
C5ΔVav
MOKO-C5ΔVav
MOWT-C5ΔVav

Figure 3

A

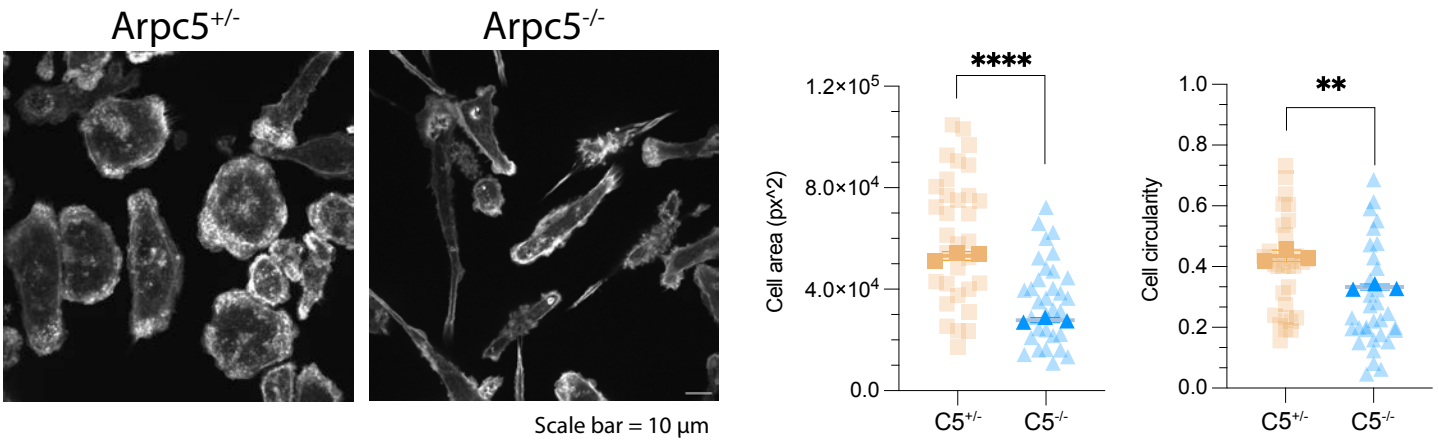

B

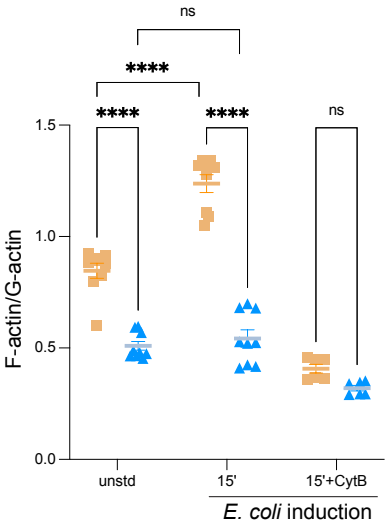

C

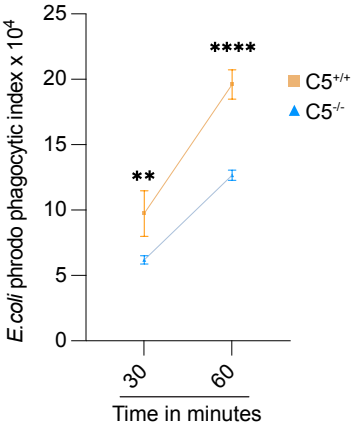

D

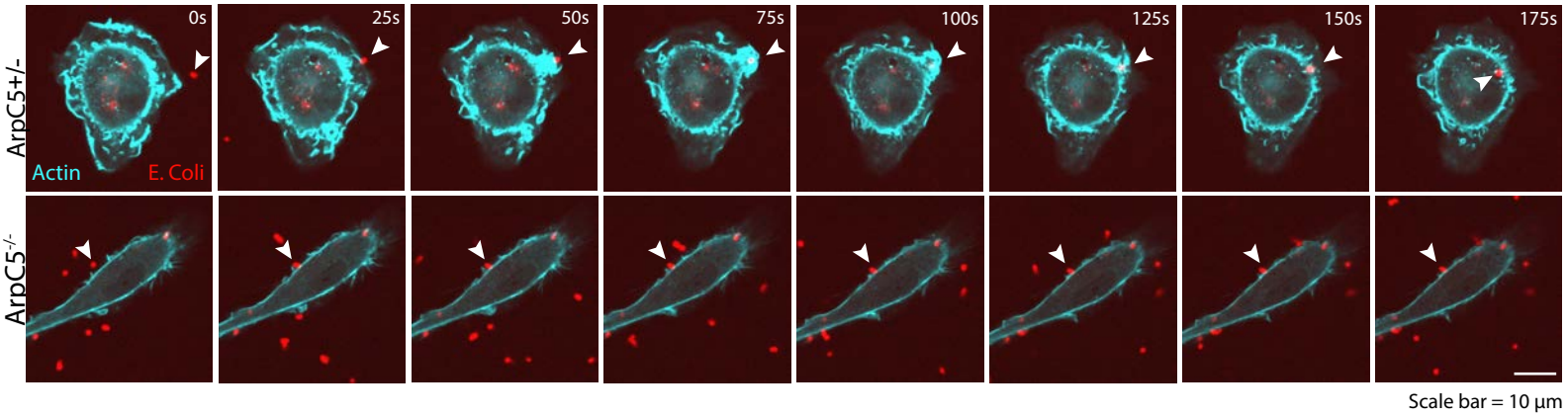

E

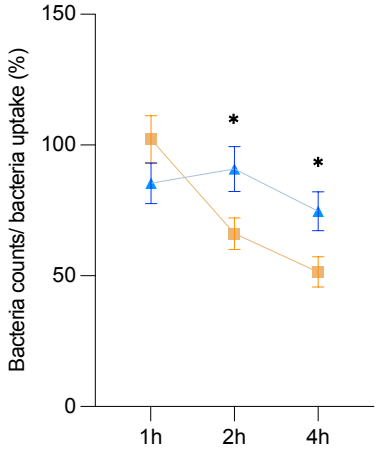

F

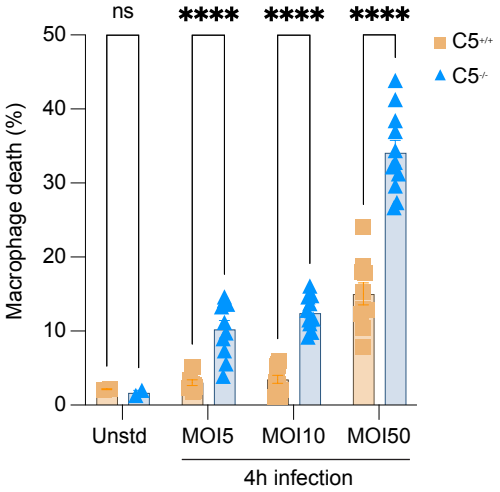

Figure 4